Hard x-ray photoemission spectroscopy of the ferrimagnetic series Gd6(Mn1–xFex)23

Truc Ly Nguyen, Thomas Mazet, Daniel Malterre, Hong Ji Lin, Masato Yoshimura, Yen Fa Liao, Hirofumi Ishii, Nozomu Hiraoka, Yuan-Chieh Tseng, Ashish Chainani

Hard x-ray photoemission spectroscopy of the ferrimagnetic series $Gd_6(Mn_{1-x}Fe_x)_{23}$

T. Ly Nguyen,[1,2] Th. Mazet,[3] D. Malterre,[3] H. J. Lin,[2] M. Yoshimura,[2] Y. F. Liao,[2] H. Ishii,[2] N. Hiraoka,[2] Y. C. Tseng,[1,4] and A. Chainani[2]

[1]*International College of Semiconductor Technology, National Yang Ming Chiao Tung University, Hsinchu 30010, Taiwan*
[2]*National Synchrotron Radiation Research Center, Hsinchu 30076, Taiwan*
[3]*Université de Lorraine, CNRS, Institut Jean Lamour, F-54000 Nancy, France*
[4]*Department of Materials Science and Engineering, National Yang Ming Chiao Tung University, Hsinchu 30010, Taiwan*

(Received 22 March 2022; revised 23 May 2022; accepted 18 July 2022; published 28 July 2022)

We study the evolution of the electronic structure of the intermetallic series $Gd_6(Mn_{1-x}Fe_x)_{23}$, $x = 0.0$–0.75, which shows nonmonotonic ferrimagnetic ordering temperatures T_C but with a systematic reduction of the total bulk magnetization upon increasing Fe content, x. We have carried out hard x-ray photoemission spectroscopy to elucidate the relation between electronic structure and properties of the series. The Gd $3d$ and Gd $4d$ core-level spectra indicate trivalent Gd^{3+} multiplets in the intermediate-coupling scheme with features due to L-S and j-J coupling. The Fe $2p$ core levels show asymmetric single peak metal-like spectra, while the Mn $2p$ core levels show asymmetric doublet peaks. The relative intensities of the Mn $2p$ doublets as a function of x indicate occupancy changes of distinct crystallographic sites associated with Mn up-spin and down-spin states. The valence band spectra identify the Gd $4f$ states at high binding energies (~7.4 eV). The Mn $3d$ states occur at the Fermi level and as a broad feature between 2 and 5 eV binding energy in Gd_6Mn_{23}. Upon substitution, the Fe $3d$ states show up as small shifts to higher binding energies compared to Mn $3d$ states. The Fe $3s$ and Mn $3s$ spectra show exchange split peaks, allowing an estimate of the Mn and Fe magnetic moments using a Van Vleck analysis, which also provides a quantification of occupancy changes with x. The overall results are consistent with the bulk net magnetization, indicating that Mn up-spin sites become Fe down-spin sites on substitution, while the nonmonotonic T_C originates in a change from Mn sublattice to Fe sublattice derived ordering.

DOI: 10.1103/PhysRevB.106.045144

I. INTRODUCTION

Understanding the properties of binary and ternary materials containing rare earths (R) and transition metals (M), which arise from an interplay of f and d electrons, remains one of the most challenging topics of condensed matter physics. The R-M based materials attracted enormous attention in the 20th century, leading to important discoveries of applied materials such as the magnets $SmCo_5$ [1] and $Nd_2Fe_{14}B$ [2]. More recently, there is a resurgence of interest in R-M based materials as they are increasingly used in permanent magnets, phosphors, lasers, energy storage batteries, catalysts, etc. [3].

R-M based materials have played and continue to play a very important role for applied magnetic materials as well as basic scientific concepts in the field of heavy fermions [4–6], non-Fermi liquids [7], magnetic metals [5–9], magnetocaloric materials [10], etc. The R-site f electrons in intermetallic alloys often behave like localized electrons with a large magnetic moment. The f electrons show large magnetic anisotropy, large spin-orbit coupling, but weak intersite exchange interactions [8,9]. This can lead to important properties such as giant magnetoresistance, large magnetocaloric effect, and colossal magnetostriction [8–10]. In contrast, the M-site d electrons are often delocalized in intermetallics and show small magnetic anisotropy, small spin-orbit coupling, but larger intersite exchange interactions. This implies the magnetic ordering temperature is often determined by the M-site moments while the total magnetization has significant contribution from both M-site and R-site moments, depending on the number of M and R atoms per unit cell. It is well known that in R_xM_y intermetallics, the R-M exchange coupling is always ferromagnetic when R is a light rare earth and antiferromagnetic when R is a heavy rare earth [11,12]. A very important aspect in R-M based materials then involves the competition of ferromagnetism vs antiferromagnetism arising from different sublattices. In this work, we investigate the role of f and d electrons in the R-M-M' ferrimagnetic series $Gd_6(Mn_{1-x}Fe_x)_{23}$, which has attracted recent interest for magnetic cooling applications [13–18].

The intermetallic compounds R_6Mn_{23} exhibit the Th_6Mn_{23} (also called G phase) type crystal structure and have attracted significant attention for their magnetic properties since 1965 [11,19–33], and more recently for their magnetocaloric properties [13–18]. Their magnetic structure exhibits an interesting and unusual coupling between the $4f$ and the $3d$ magnetic moments [14,19,27,30]. While an early study concluded that the R_6Mn_{23} compounds were apparent exceptions in terms of R-M exchange coupling for the light and heavy rare earths [19], a subsequent study showed that the Mn sites exhibited a complex magnetic structure [27]. From polarized

neutron diffraction results for isostructural Y_6Mn_{23} at 4.2 K, it was shown that the magnetic moments of Mn atoms on the b ($\sim -2.8\mu_B$) and d sites ($\sim -2.1\mu_B$) are oriented antiparallel to those on the f_1 ($\sim +1.8\mu_B$) and f_2 ($\sim +1.8\mu_B$) sites [27]. Accordingly, it was concluded that there are two types of Mn spin sites: up-spin "f_1, f_2" sites ($\equiv A$ site), and down-spin "b, d" sites ($\equiv B$ site) in Y_6Mn_{23}. In contrast, in Y_6Fe_{23}, the Fe moments are oriented along the same direction for all four M sites (b, d, f_1, f_2) and can be represented by one type of Fe with an average value of magnetic moment of $\sim +1.94\mu_B$ [29,34]. Based on this complex magnetic structure with the Mn sublattice itself being ferrimagnetic, and the R moments interacting more strongly with the "b, d" sites compared to the "f_1, f_2" sites, it was possible to resolve the apparent exception of R_6Mn_{23} compounds [14,27].

Early studies showed that upon Fe substitution in Y_6Mn_{23}, the net magnetization of isostructural $Y_6(Mn_{1-x}Fe_x)_{23}$ compounds increases with increasing x. However, in isostructural $Gd_6(Mn_{1-x}Fe_x)_{23}$ compounds, the net magnetization reduces upon increasing x [13,17,22,26,29,32]. In contrast, the behavior of T_C in $Y_6(Mn_{1-x}Fe_x)_{23}$ compounds is nonmonotonic and similar to the $Gd_6(Mn_{1-x}Fe_x)_{23}$ compounds [13,22,32]. The parent compounds showed large values of $T_C \sim 500$ K, but the T_C reduces for small Fe content, and then increases for rich Fe content. Specifically, $Gd_6(Mn_{1-x}Fe_x)_{23}$ showed a lowest $T_C = 120$ K for $x = 0.5$ [22], while $T_C = 489$ K for $x = 0.0$ and 467 K for $x = 1.0$ [17,22]. These results suggested that T_C of these compounds does not depend on the R elements in the compounds, but is derived from transition metal moments. Magnetocaloric results of $Gd_6(Mn_{1-x}Fe_x)_{23}$ showed two maxima in the magnetic entropy changes (ΔS_M) as a function of temperature, one at T_C and the other at $T \sim 100$ K. It was suggested that the maximum at $T \sim 100$ K could be associated with the magnetic ordering of the Gd sublattice or it arose from modifications in the magnetic structure with small Fe content ($x = 0.0$–0.2) [13].

Although the structural, electrical, magnetic, and magnetocaloric properties of $Gd_6(Mn_{1-x}Fe_x)_{23}$ were investigated extensively [13,17,22,26,29,32], photoemission spectroscopy studies for relating electronic structure with properties in $Gd_6(Mn_{1-x}Fe_x)_{23}$ compounds have not been reported to date. Recent studies of Gd $3d$ and $4d$ spectra of Gd intermetallics [35,36] measured with bulk sensitive hard x-ray photoemission spectroscopy (HAXPES) showed very clear multiplet features. It is noted that at the sample surface, the binding energies of the valence $4f$ levels and core levels can show surface level shifts relative to the bulk, which can lead to apparently poorer resolution of the Gd multiplets. Further, the structural and magnetic properties in the near surface region can deviate from the bulk, so it is better to use the highest possible bulk sensitivity which is obtained by using high photon energies. Hence, we have carried out bulk sensitive HAXPES [37] to investigate the electronic states of the series $Gd_6(Mn_{1-x}Fe_x)_{23}$. We have carried out composition (x)-dependent HAXPES to characterize the core levels of Gd $3d, 4d$, Mn $2p, 3p, 3s$, and Fe $2p, 3p, 3s$, as well as the valence band occupied states. The Mn $3s$ and Fe $3s$ spectra were analyzed to estimate the spin magnetic moments of Mn and Fe. The results provide us an understanding of the electronic structure of the series $Gd_6(Mn_{1-x}Fe_x)_{23}$ and its relation with their structural occupancy changes and magnetic properties. The overall results provide an explanation for the bulk net magnetization, and the origin of nonmonotonic T_C is associated with a change from Mn sublattice to Fe sublattice derived ordering.

II. SAMPLE PREPARATION, CHARACTERIZATION, AND EXPERIMENTAL DETAILS

The $Gd_6(Mn_{1-x}Fe_x)_{23}$ compounds with $x = 0$, 0.2, 0.3, 0.5, and 0.75 were synthesized from stoichiometric amounts of high-purity elements (Gd 99.9 wt % from Rhodia, Mn 99.99 wt % from Cerac, and Fe 99.8 wt % from Alfa Aesar). The mixtures were melted in a water-cooled copper crucible using a high frequency induction furnace (CELES) under pure argon atmosphere. The purity and chemical composition of each sample have been checked by microprobe analysis (Cameca SX 100) on mirror polished powder samples dispersed in a cold resin. The purity was evaluated from backscattered electron micrographs on different particles and the chemical composition was determined from an average of six pinpoints randomly chosen among the sample. The crystallographic structure and the presence of impurities have been verified by powder x-ray diffraction (Philips X'Pert Pro Diffractometer, Cu $K\alpha$) [13,38].

The HAXPES experiments were carried out on a spectrometer with a total-energy resolution of 280 meV at the Taiwan beam line BL12XU in SPring-8, Hyogo, Japan using linearly polarized photons. The sample was cooled using a liquid-N_2 flow-type cryostat. Samples were cleaved in the preparation chamber in a vacuum of 5×10^{-9} mbar and immediately transferred for measurements in the main chamber at $T = 80$ K at a vacuum of 5×10^{-10} mbar. The energy calibration and resolution were determined from the Fermi-edge (E_F) spectrum of a gold film evaporated on the sample holder. The HAXPES data were obtained in the angle-integrated mode with an incident photon energy $h\nu = 6.5$ keV. The Gd $3d$ and Gd $4d$ as well as $2p$ and $3s$ core-level spectra of Fe and Mn in the series were fitted using a least-squares method to quantify peak-energy positions and widths. The fits shown in this work used a Shirley-type background with asymmetric Doniach-Sunjic type Voigt profiles for all peaks. The Shirley-type background is based on the simple assumption that the probability of secondary energy losses is independent of the magnitude of the energy loss, and accordingly, the background at a given kinetic energy position E is proportional to the integral of all higher kinetic energy spectral intensities.

III. RESULTS AND DISCUSSION

A. Core-level and valence band HAXPES

The Gd $3d$ core-level HAXPES spectra of $Gd_6(Mn_{1-x}Fe_x)_{23}$ measured with an incident photon energy $h\nu = 6.5$ keV at $T = 80$ K are shown in Fig. 1. Figure 1(a) shows the full range Gd $3d$ spectrum for $x = 0$. The spectrum shows two main regions which can be assigned to spin-orbit coupling derived $3d_{5/2}$ and $3d_{3/2}$ states. Figures 1(b) and 1(c) show the expanded scale regions of Gd $3d_{5/2}$ and Gd $3d_{3/2}$ for all x, in order to clarify the detailed features. The spectra are very similar to recently reported Gd $3d$ studies using

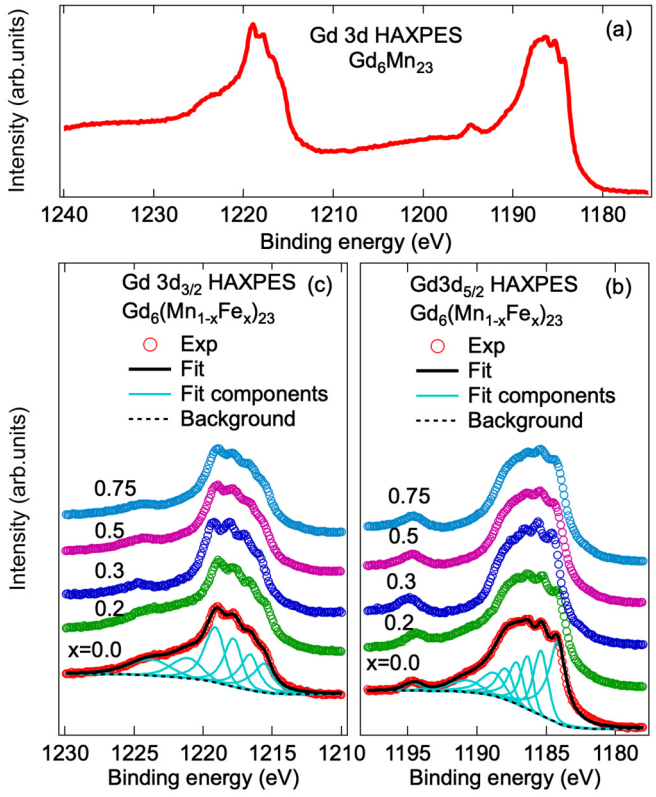

FIG. 1. The Gd 3*d* core-level HAXPES experimental spectra of $Gd_6(Mn_{1-x}Fe_x)_{23}$, $x = 0.0$, 0.2, 0.3, 0.5, and 0.75, measured at $T =$ 80 K. (a) The full range Gd 3*d* core-level HAXPES experimental spectrum of Gd_6Mn_{23}. (b) shows the Gd $3d_{5/2}$ states and (c) shows the Gd $3d_{3/2}$ states on an expanded scale, along with the curve fit for $x = 0.0$ using a least-squares method. The fitting parameters are listed in Table I.

HAXPES. These studies reported HAXPES for amorphous GdFe [35] and crystalline GdNi [36] and showed that the

TABLE I. Fitting parameters for the Gd 3*d* core-level spectrum, with component peaks listed from lowest binding energy to highest binding energy.

Component peaks Gd $3d_{5/2}$	Fitted peaks eV (±0.1)	FWHM eV (±0.1)
1 ($J' = 6$)	1184.2	1.4
2 ($J' = 5$)	1185.4	1.2
3 ($J' = 4$)	1186.4	1.0
4 ($J' = 3$)	1187.1	1.1
5 ($J' = 2$)	1187.9	1.2
6 ($J' = 1$)	1188.8	1.8
7 (J'_{sat})	1190.7	2.4
8 (^7D)	1194.6	1.4
Gd $3d_{3/2}$	eV (±0.1)	eV (±0.1)
1 ($J' = 2$)	1215.6	1.5
2 ($J' = 3$)	1216.6	1.4
3 ($J' = 4$)	1217.8	1.4
4 ($J' = 5$)	1219.1	1.5
5 (J'_{sat})	1221.1	2.4
6 (^7D)	1223.7	3.2

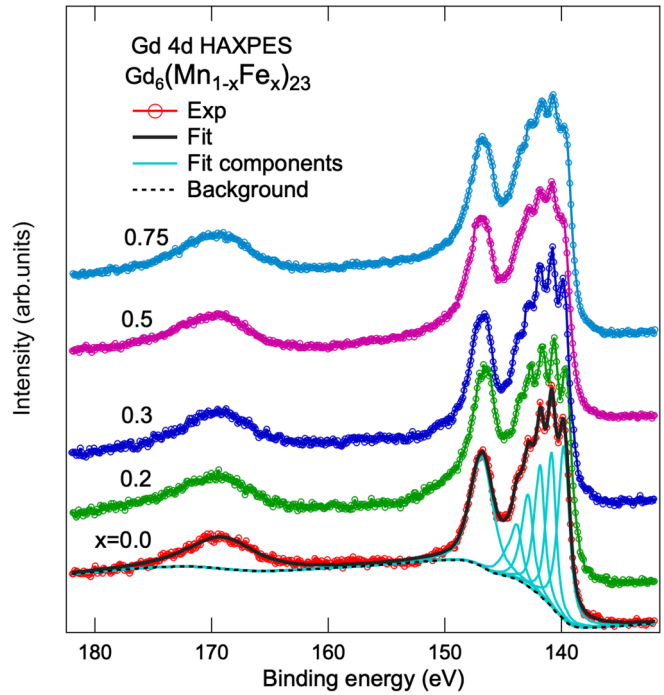

FIG. 2. The Gd 4*d* core-level HAXPES experimental spectra of $Gd_6(Mn_{1-x}Fe_x)_{23}$, $x = 0.0$, 0.2, 0.3, 0.5, and 0.75, measured at $T =$ 80 K. The parent Gd_6Mn_{23} ($x = 0.0$) spectrum was fitted by using a least-squares method and the fitting parameters are listed in Table II.

Gd 3*d* spectra can be analyzed in terms of the atomic multiplets of Gd^{3+} obtained in the intermediate coupling scheme with features due to *L*-*S* and *j*-*J* coupling. The main peak of Gd $3d_{5/2}$ [spread between 1182 and 1190 eV binding energy (BE)] and Gd $3d_{3/2}$ (spread between 1215 and 1220 eV BE) show features corresponding to ^9D states and the lower intensity high BE features at 1194.58 and 1223.75 eV are the ^7D features. The $3d_{5/2}$ multiplets arise from the $J = 7/2$ state coupling with the $j = 5/2$ core hole and result in multiplets of total angular momentum $J' = 6, 5, 4, 3, 2, 1$ with approximate multiplicities of $2J' + 1$. The lowest BE state is the $J' = 6$ final state with the 3*d* spin and orbital momenta parallel to the 4*f* spin moment. Similarly, the $J = 7/2$ state couples to the $j = 3/2$ core hole and results in multiplets of total angular momentum $J' = 5, 4, 3, 2$. Here, the $J' = 2$ final state has the lowest BE with 4*f* and 3*d* spin moments parallel, but oriented opposite to the 3*d* orbital moment. These assignments of Gd 3*d* multiplets in the intermediate-coupling scheme were validated by comparing the atomic multiplet calculations with experimental spectra [35,36]. In addition, the atomic multiplet calculations showed a small peak at a BE of 1190.68 eV and 1221.10 eV BE between the ^9D and ^7D features [36]. Based on these assignments, we have carried out a least-squares fit to the data as shown in Figs. 1(b) and 1(c) which reiterates the assignment of the atomic multiplets. The similarity of Gd 3*d* spectra in the series indicates the trivalent state of Gd ions in the entire $Gd_6(Mn_{1-x}Fe_x)_{23}$ series.

The Gd 4*d* core-level HAXPES spectra of $Gd_6(Mn_{1-x}Fe_x)_{23}$ compounds measured at $T = 80$ K are shown in Fig. 2. Just like the analysis for the Gd 3*d* spectra,

TABLE II. Fitting parameters for the Gd 4*d* core-level spectrum, with component peaks listed from lowest binding energy to highest binding energy.

Component peaks Gd 4*d*	Fitted peaks eV (±0.1)	FWHM eV (±0.1)
1 ($J' = 6$)	139.8	1.1
2 ($J' = 5$)	140.9	0.9
3 ($J' = 4$)	141.8	0.9
4 ($J' = 3$)	142.9	1.1
5 ($J' = 2$)	143.9	1.1
6 ($^7D_1$)	146.8	2.3
7 ($^7D_5$)	169.1	6.8

the Gd 4*d* spectra can also be analyzed in terms of the Gd 4*d* atomic multiplets of the Gd^{3+} state in the intermediate coupling scheme, as was shown in early studies of Gd metal and Gd intermetallics [36,39–42]. Accordingly, the Gd $4d^9$ (^2D) hole state couples to the $4f^7$ (^8S) state, resulting in ^9D and ^7D final states. The ^9D states split into five multiplet peaks with $J' = 6, 5, 4, 3, 2$. Similarly, the ^7D states will also split into five levels $J' = 5, 4, 3, 2, 1$, but since the ^7D states can couple to not only the ^8S term of $4f^7$, but also to the higher energy terms ^6P, ^6D, ^6F, and ^6G states of $4f^7$, the Coulomb and exchange interaction results in a strong modification of the five-peak pattern. This results in the lowest BE $^7D_1$ state at 146.83 eV and the highest BE $^7D_5$ state at 169.07 eV, while the $^7D_2$, $^7D_3$, and $^7D_4$ states are not observed due to very low spectral intensities of less than 0.1%, as was reported also for Gd metal [36,41,42]. The Gd 4*d* main peak could be accordingly fitted with five peaks corresponding to $J' = 6, 5, 4, 3, 2$ for the ^9D final states and one peak each for the $^7D_1$ and $^7D_5$ features of the ^7D final states. The results again confirm that Gd ion in all the compounds can be described as Gd^{3+} states.

We have next carried out the Mn 2*p* core-level HAXPES measurements of $Gd_6(Mn_{1-x}Fe_x)_{23}$ at $T = 80$ K as shown in Fig. 3. The spectra show two main peaks corresponding to the $2p_{3/2}$ and $2p_{1/2}$ spin-orbit splitting with BE of 638.42 and 649.72 eV, respectively. The main peak BE of 638.42 eV matches the Mn metal BE [43]. The absence of satellite features between 4 and 8 eV higher BEs compared to the main peak indicates the absence of oxidation. However, a shoulder feature is observed at about 1 eV higher BE to the $2p_{3/2}$ and $2p_{1/2}$ main peaks, and its relative intensity compared to the main peak changes with Fe content for all x. We carried out a least-squares fitting of the spectra using Doniach-Sunjic line shapes to quantify the relative intensities of the metallic peaks. We have tried fits using a Tougaard background or a Shirley background, and found that we needed larger asymmetry parameters when using a Tougaard background. Since we wanted a more strict confirmation of the asymmetry to justify metallic peak shape, we used a Shirley background for all the peak fits. The results indicate that the main and shoulder peak intensities match fairly well with the relative occupancies of the *A* and *B* sites of Mn as estimated from neutron diffraction [26,27], as well as our estimates of magnetic moments from 3*s* core levels discussed in Sec. III B. Accordingly, we have assigned the main peak and shoulder

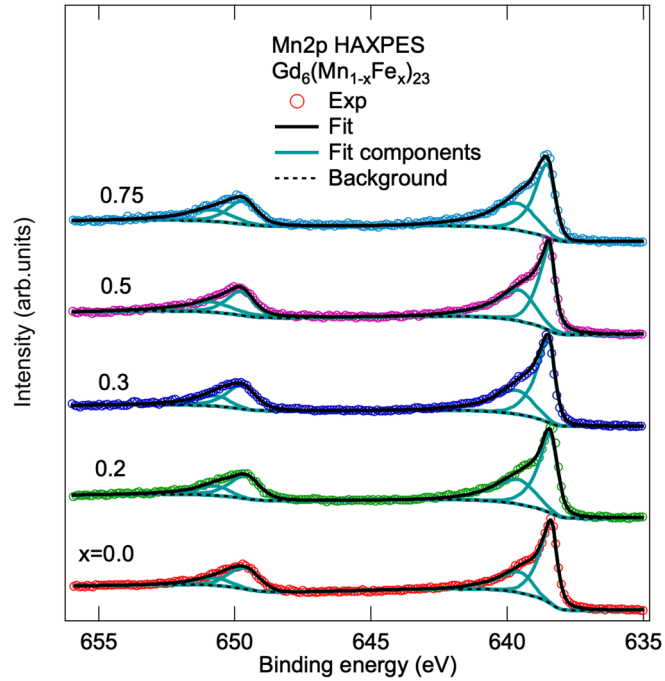

FIG. 3. The Mn 2*p* core-level HAXPES spectra of $Gd_6(Mn_{1-x}Fe_x)_{23}$, $x = 0.0$, 0.2, 0.3, 0.5, and 0.75, measured at $T = 80$ K.

to metal-like features associated with the *A* and *B* sites, respectively.

The Fe 2*p* core-level HAXPES experimental spectra of $Gd_6(Mn_{1-x}Fe_x)_{23}$ are shown in Fig. 4. The spectra exhibit single peaks positioned at BEs of 706.88 and 719.78 eV

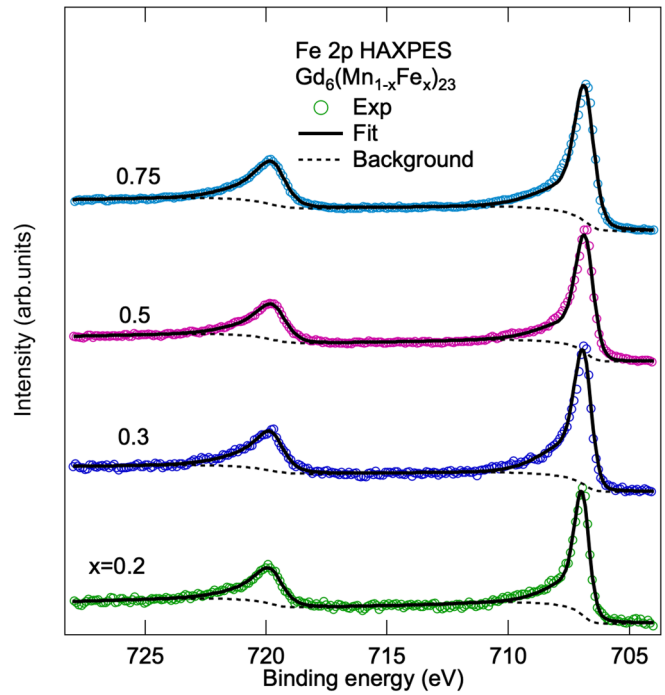

FIG. 4. The Fe 2*p* core-level HAXPES spectra of $Gd_6(Mn_{1-x}Fe_x)_{23}$, $x = 0.0$, 0.2, 0.3, 0.5, and 0.75, measured at $T = 80$ K.

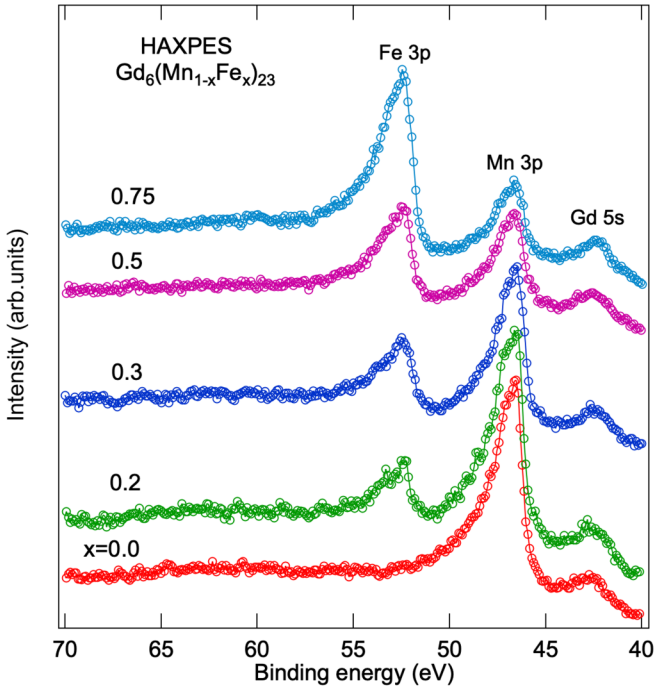

FIG. 5. The Mn 3p and Fe 3p core-level HAXPES spectra of $Gd_6(Mn_{1-x}Fe_x)_{23}$, $x = 0.0$, 0.2, 0.3, 0.5, and 0.75, measured at $T = 80$ K.

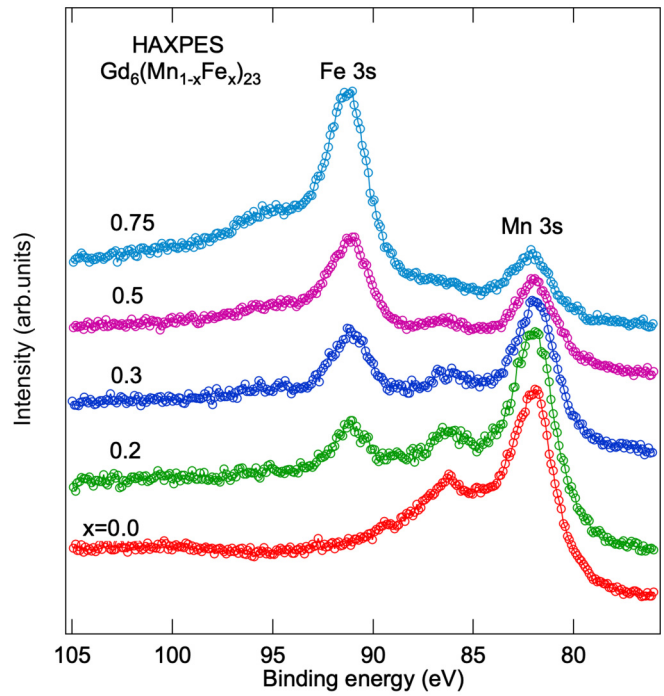

FIG. 6. The Mn 3s and Fe 3s core-level HAXPES experimental spectra of $Gd_6(Mn_{1-x}Fe_x)_{23}$, $x = 0.0$, 0.2, 0.3, 0.5, and 0.75, measured at $T = 80$ K.

corresponding to the spin orbit split $2p_{3/2}$ and $2p_{1/2}$ feature, respectively. The BEs of the peaks match with Fe metal [43] and confirm the metal-like core level of Fe in the series.

Figure 5 shows the Mn 3p and Fe 3p core-level HAXPES experimental spectra of $Gd_6(Mn_{1-x}Fe_x)_{23}$ measured at $T = 80$ K. The spectra also show a weak Gd 5s feature at 42.73 eV BE [44] along with the Mn 3p at 46.63 eV BE and Fe 3p at 52.33 eV BE. By normalizing the spectral intensity of the Gd 5s feature, the relative intensity of Mn 3p and Fe 3p shows a very systematic behavior. Namely, the intensity of the Mn 3p is reduced while Fe 3p is increased, proportional to the Fe substitution. A similar behavior for the relative intensities of the Mn 3s and Fe 3s core-level HAXPES spectra changing with x is also obtained for the series, as shown in Fig. 6. Thus, by increasing the Fe content, the intensity of Mn 3s spectra is reduced and Fe 3s is enhanced, consistent with Mn and Fe concentrations. Further, the Mn 3s and Fe 3s spectra show a broad main peak and exchange-split satellites which are due to the local moment of Mn and Fe in $Gd_6(Mn_{1-x}Fe_x)_{23}$. The Mn 3s and Fe 3s spectra are discussed later in more detail in relation to the analysis of the Mn and Fe magnetic moments.

Figure 7 presents the wide valence band HAXPES spectra of $Gd_6(Mn_{1-x}Fe_x)_{23}$ measured at 80 K. The spectra show a high intensity feature at 7.4 eV BE which is due to Gd 4f states, and all the spectra are normalized to this feature. For Gd_6Mn_{23}, the states between 0 and ~5 eV BE consist of one broad feature between 2 and 5 eV and a narrower feature at and near E_F which are attributed to Mn 3d states. The broad feature between 2 and 5 eV shows small changes upon Fe substitution. As can be seen by superimposing the Fe $x = 0.75$ spectrum (blue squares) on the $x = 0.0$ spectrum (red circles), the Fe 3d states show up at slightly higher BEs compared to the Mn 3d states. The near E_F feature which is sharp in Gd_6Mn_{23} becomes a little broader for Fe substituted compositions on the higher BE side with a small intensity reduction at E_F. It is noted that, based on band structure

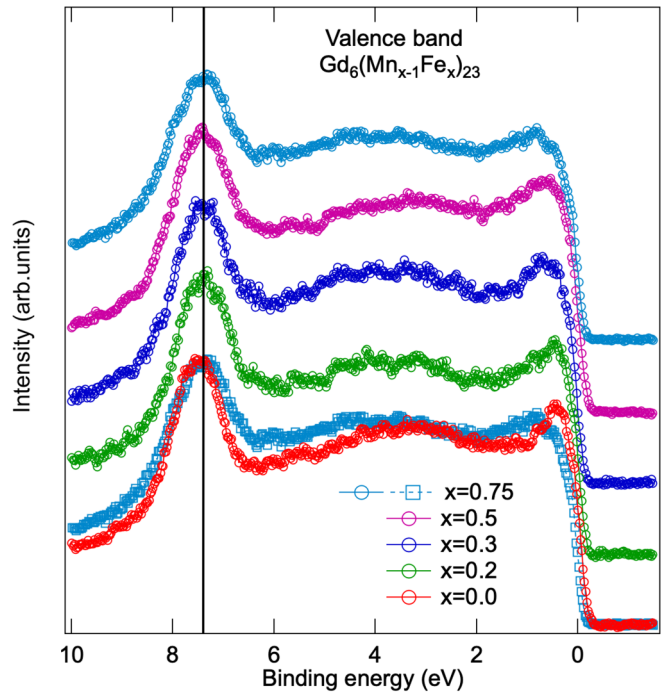

FIG. 7. The valence band HAXPES experimental spectra of $Gd_6(Mn_{1-x}Fe_x)_{23}$, $x = 0.0$, 0.2, 0.3, 0.5, and 0.75, measured at $T = 80$ K.

TABLE III. Mn and Fe occupancies of A and B sites from the 3s HAXPES fitting.

	Mn atoms			Fe atoms		
Fe content (x)	$(A+B)_{Mn}$ no. from x	A_{Mn} no. (±0.05)	B_{Mn} no. (±0.05)	$(A+B)_{Fe}$ no. from x	A_{Fe} no. (±0.05)	B_{Fe} no. (±0.05)
0.0	23	15.93 (100%)	7.05 (100%)	0	0	0
0.3	16.1	9.16 (59%)	6.94 (98%)	6.9	6.84 (99%)	0.06 (1%)
0.5	11.5	6.15 (39%)	5.35 (76%)	11.5	9.85 (86%)	1.65 (14%)
0.75	5.75	3.26 (20%)	2.49 (35%)	17.25	12.74 (74%)	4.51 (26%)

calculations of Gd based R-M intermetallics [45], Gd 5d states are also expected to contribute at and near E_F, overlapping with the Mn 3d and Fe 3d states in the present case. Similar behavior with broad M 3d split band states spread between E_F and ∼5 eV BE and Gd 4f states at ∼7.5 eV BE have been reported for several Gd-containing intermetallics [46–51].

B. 3s analysis for magnetic moments

It is known that the spin magnetic moment of a transition metal 3d element can be estimated from 3s photoemission spectra. Based on the Van Vleck model [52], the ratio of the intensities of the 3s main peak and exchange-split satellite can be written as [53–59] $I_m/I_s = (S+1)/S$, where S is the spin quantum number, I_m is the intensity of the main peak, and I_s is the intensity of the exchange-split satellite. The spin magnetic moment is given by $\mu_{spin} = 2\mu_B\sqrt{S(S+1)}$. It is noted that

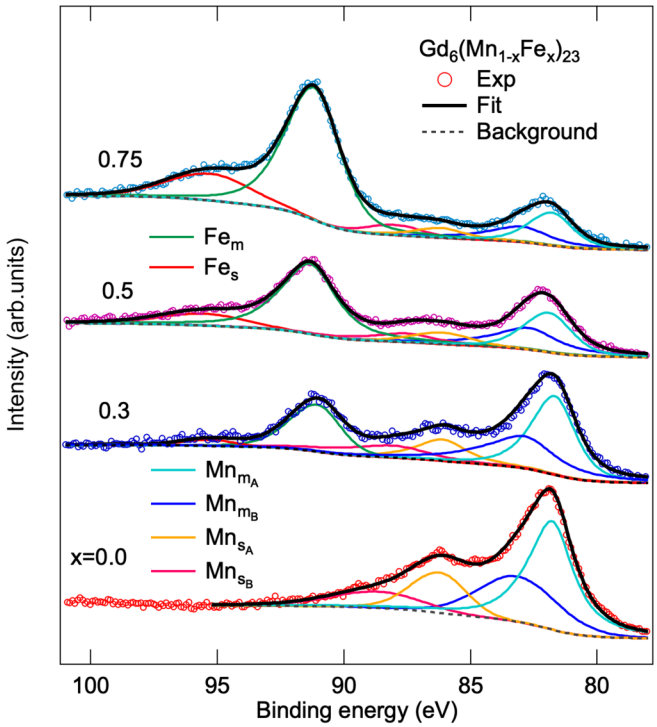

FIG. 8. The Mn 3s and Fe 3s core-level HAXPES spectra of $Gd_6(Mn_{1-x}Fe_x)_{23}$ for $x = 0.0$, 0.3, 0.5, and 0.75 were fitted by using a least-squares method. The Mn 3s consists of two main peaks "m_A, m_B" and exchange-split satellites "s_A, s_B," while the Fe 3s consists of one main peak "m" and one exchange-split satellite "s."

while the Van Vleck model works reasonably well for intermetallics [51,55,56], more recent studies have shown that a sum rule method is a better way to investigate the exchange energy in the 3s spectra of ionic compounds with well-defined d^n configurations [54,57–59]. Since we cannot assign a proper electron configuration or valency to Fe and Mn states in intermetallic alloys, we have used the simpler Van Vleck model to determine the magnetic moment via the ratio of the main and satellite peak intensities of the 3s spectra. We first discuss the spin magnetic moment analysis for Gd_6Mn_{23}. The Mn 3s spectra of Gd_6Mn_{23} could be fitted with four peaks consisting of two main peaks "m_A, m_B" and two exchange-split satellites "s_A, s_B," as shown in Fig. 8. The two pairs indicate that the Mn atoms show two distinct spin moments. Further, the two main peaks show intensities proportional to the number of A-site (16 atoms) and B-site (7 atoms) Mn atoms, corresponding to the "f_1, f_2" sites and the "b, d" sites known from the neutron diffraction results. By applying the Van Vleck equations, we obtained spin magnetic moments for the A site and B site to be $1.77 \pm 0.05\mu_B$ and $2.25 \pm 0.05\mu_B$, respectively. This result is very close to the occupancy and magnetic moments obtained from neutron diffraction studies [27].

TABLE IV. The values of μ_{spin} obtained for Mn and Fe from the 3s analysis.

$x = 0.0$	ΔE eV (±0.15)	I_m/I_s (±0.03)	S (±0.03)	μ_{spin} μ_B (±0.05)
Mn (f_1, f_2)	4.44	2.94	0.52	+1.77
Mn (4b, 24d)	5.51	2.73	0.73	−2.25
$x = 0.3$				
Mn (f_1, f_2)	4.41	3.03	0.49	+1.71
Mn (4b, 24d)	5.2	2.36	0.74	−2.26
Fe	4.08	9.67	0.11	−0.71
$x = 0.5$				
Mn (f_1, f_2)	4.18	3.00	0.50	+1.73
Mn (4b, 24d)	4.84	2.45	0.69	−2.16
Fe	4.15	4.99	0.25	−1.12
$x = 0.75$				
Mn (f_1, f_2)	4.17	2.82	0.55	+1.84
Mn (4b, 24d)	5.00	2.38	0.72	−2.23
Fe	4.08	3.73	0.37	−1.41

TABLE V. Comparison of total magnetization.

		3*s* analysis (this work)	Lemoine result (Ref. [13])	Kirchmayr result (Ref. [22])	Nagai result (Ref. [32])
Fe content	T_C	Net M	9 T	1 T	1 T
(x)	(K)	(μ_B)	(μ_B)	(μ_B)	(μ_B)
0	489 ±5 [13]	54.2 ± 3.0	54.7±2.0	50 ±2	40 ±4
0.3	142 ±5 [22]	36.7 ± 3.0		35 ±2	28 ±4
0.5	120 ±5 [22]	28.8 ± 3.0		30 ±2	26 ±4
0.75	309 ±5 [13]	17.6 ± 3.0	16.2±2.0	20.4±2	15 ±3

Similarly, we have carried out least-squares fits of the Mn 3*s* and Fe 3*s* spectra for $x = 0.3$, 0.5, and 0.75 in order to estimate their occupancies and magnetic moments, as shown in Fig. 8. The Fe 3*s* spectra were fitted with a single main peak and satellite, while the Mn 3*s* spectra were fitted with doublets. For $x = 0.2$, we could not make a reliable estimate of the magnetic moments due to the negligible intensity for the Fe 3*s* exchange-split feature and the overlap of the Fe 3*s* main peak with the Mn 3*s* exchange-split satellite (Fig. 6). From the fittings to Mn 3*s* spectra we have determined the occupancy of Mn atoms in the *A* site and *B* site as listed in Table III. Thus, obtaining the main and satellite peak intensities, we have estimated the Mn and Fe spin magnetic moments for $x = 0.3$, 0.5, and 0.75 as listed in Table IV. From the results shown in Table III, it is clear that Fe preferentially occupies the *A* sites compared to the *B* sites upon substitution. For $x = 0.3$, 99% of the Fe atoms go to the *A* site, while for $x = 0.5$ and 0.75, it gets slightly reduced to 86% and 74%, respectively, with a corresponding increase in the *B*-site occupancy. It is interesting to compare the occupied percentage of Mn up-spin and down-spin sites relative to the total number of Mn *A* and Mn *B* sites, respectively, as listed in Table III. The results suggest that the preferential reduction of available Mn *A* sites leads to the increase of occupancy of Fe *B* sites for $x \geqslant 0.5$.

Table V shows the total net magnetization M from the 3*s* analysis according to the formula $M = 6\mu_{\mathrm{Gd}} + 23[(1 - x)\mu_{\mathrm{Mn}} + x\mu_{\mathrm{Fe}}]$, where μ_{Mn} and μ_{Fe} are magnetic moments obtained from 3*s* analysis, and the gadolinium ion spin moment of Gd^{3+} was taken to be the free-ion value of $\mu_{\mathrm{Gd}} = +7\mu_B$. The obtained values of the total net magnetization M are compared with the bulk magnetization results from earlier work [13,22,32] in Table V and also plotted in Fig. 9. The values of total net magnetization M are in good agreement with the results of bulk magnetization if, and only if, we consider the *A*-site and *B*-site Mn moments are parallel and antiparallel to the Gd moments, respectively, and the *A*- and *B*-site Fe moments are both antiparallel to the Gd moments. In particular, the estimated magnetization values are within error bars with the bulk magnetization values reported by Lemoine *et al.* [13] and Kirchmayr and Steiner [22], while the values reported by Nagai *et al.* [32] are consistently lower. The results are thus fairly consistent with the known bulk net magnetization results, and confirm that Mn up-spin sites become Fe down-spin sites on substitution. Since the $Gd_6(Mn_{1-x}Fe_x)_{23}$ series shows a minimum $T_C = 120$ K for $x = 0.5$ [22], the estimated magnetic moments for Mn and Fe indicate that the Fe down-spin moments replacing the Mn up-spin moments are responsible for the nonmonotonic T_C behavior, which corresponds to a change from Mn sublattice to Fe sublattice derived ordering.

IV. CONCLUSIONS

In conclusion, the electronic structure of $Gd_6(Mn_{1-x}Fe_x)_{23}$ was investigated using HAXPES. The Gd 3*d* and Gd 4*d* core-level spectra indicate trivalent Gd^{3+} states which exhibit multiplets in the intermediate-coupling scheme. The Mn 2*p* spectra show two metal-like features attributed to "*b*, *d*" and "f_1, f_2" sites, and their relative intensities change with x while Fe 2*p* spectra show only a single metal-like feature. The

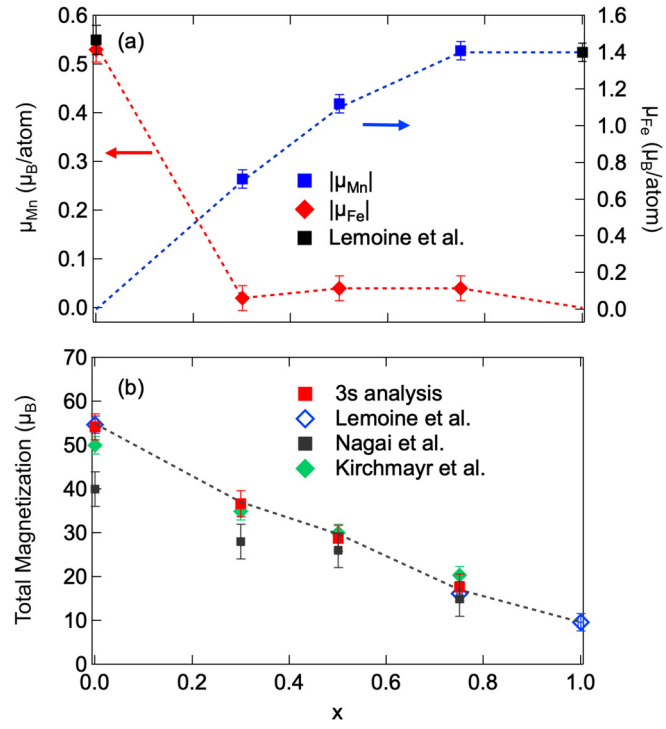

FIG. 9. A summary of (a) the magnetic moments of Fe and Mn as well as (b) the total magnetization as a function of x, compared to earlier reports. The systematic increase in Fe moments results in a systematic decrease in the total net magnetization of $Gd_6(Mn_{1-x}Fe_x)_{23}$.

relative intensities of the Mn $2p$ doublets show occupancy changes of distinct crystallographic sites associated with Mn up-spin and down-spin states. The valence band spectra show the Gd $4f$ states at high binding energies (∼7.4 eV), away from E_F. The Mn $3d$ states occur at E_F and within 5 eV BE for Gd_6Mn_{23}, and upon substitution, the Fe $3d$ states are observed at slightly higher binding energies and with a reduced intensity at E_F, compared to Mn $3d$ states. The Fe $3s$ and Mn $3s$ spectra show exchange splitting due to local moments. The Mn and Fe magnetic moments could be estimated using a Van Vleck analysis, and the Mn and Fe site occupancies could be determined. The overall results show a systematic reduction of the net magnetization, while the origin of nonmonotonic T_C is attributed to a change from Mn sublattice to Fe sublattice derived ordering.

ACKNOWLEDGMENTS

A.C. acknowledges the Ministry of Science and Technology (MOST) of Taiwan, Republic of China for financially supporting this research under Contract No. MOST 108-2112-M-213-001-MY3. The synchrotron radiation experiments were performed at BL12XU of SPring-8 with the approval of the Japan Synchrotron Radiation Research Institute (JASRI) (Proposals No. 2020A4256 and No. 2021A4255).

[1] K. Strnat, The recent development of permanent magnet materials containing rare earth metals, IEEE Trans. Magn. **6**, 182 (1970).

[2] J. Herbst, $R_2Fe_{14}B$ materials: Intrinsic properties and technological aspects, Rev. Mod. Phys. **63**, 819 (1991).

[3] V. Balaram, Rare earth elements: A review of applications, occurrence, exploration, analysis, recycling, and environmental impact, Geosci. Front. **10**, 1285 (2019).

[4] G. R. Stewart, Heavy-fermion systems, Rev. Mod. Phys. **56**, 755 (1984).

[5] T. Mazet, D. Malterre, M. Franois, C. Dallera, M. Grioni, and G. Monaco, Nonpareil Yb Behavior in $YbMn_6Ge_{6x}Sn_x$, Phys. Rev. Lett. **111**, 096402 (2013).

[6] L. Eichenberger, A. Magnette, D. Malterre, R. Sibille, F. Baudelet, L. Nataf, and T. Mazet, Possible room-temperature signatures of unconventional $4f$-electron quantum criticality in $YbMn_6Ge_{6x}Sn_x$, Phys. Rev. B **101**, 020408(R) (2020).

[7] G. R. Stewart, Non-Fermi-liquid behavior in d- and f-electron metals, Rev. Mod. Phys. **73**, 797 (2001).

[8] K. N. R. Taylor, Intermetallic rare-earth compounds, Adv. Phys. **20**, 551 (1971).

[9] W. E. Wallace, *Rare Earth Intermetallics* (Academic, New York, 1973).

[10] S. B. Roy, Magnetocaloric effect in intermetallic compounds and alloys, in *Handbook of Magnetic Materials*, edited by K. H. J. Buschow (North-Holland, Amsterdam, 2014), Vol. 22, Chap. 2, pp. 203–316.

[11] I. A. Campbell, Indirect exchange for rare earths in metals, J. Phys. F: Met. Phys. **2**, L47 (1972).

[12] M. S. S. Brooks, T. Gasche, S. Auluck, L. Nordström, L. Severin, J. Trygg, and B. Johansson, $3d$-$5d$ band magnetism in rare earth-transition metal intermetallics: total and partial magnetic moments of the RFe_2, (R=Gd-Yb) Laves phase compounds, J. Appl. Phys. **70**, 5972 (1991).

[13] P. Lemoine, V. Ban, A. Vernière, T. Mazet, and B. Malaman, Magnetocaloric properties of $Gd_6(Mn_{1-x}Fe_x)_{23}$ alloys ($x \leqslant 0.2$), Solid State Commun. **150**, 1556 (2010).

[14] P. Lemoine, A. Verniére, T. Mazet, and B. Malaman, Magnetic and magnetocaloric properties of R_6Mn_{23} (R=Y, Nd, Sm, Gd-Tm, Lu) compounds, J. Magn. Magn. Mater. **323**, 2690 (2011).

[15] P. Lemoine, A. Vernière, T. Mazet, and B. Malaman, Magnetic and magnetocaloric properties of R_6Mn_{23} (R = Y, Sm, Tb, Dy, Ho and Er) compounds, J. Alloys Compd. **578**, 413 (2013).

[16] P. Lemoine, A. Vernière, B. Malaman, and T. Mazet, Magnetic and magnetocaloric properties of $Gd_6(Mn_{1-x}Co_x)_{23}$ compounds ($x \leqslant 0.3$), J. Alloys Compd. **680**, 612 (2016).

[17] P. Lemoine, Ph.D. thesis, Université Henri Poincaré, Nancy, 2011.

[18] P. L. Dong, L. Ma, X. Zhou, D. Wang, Q. R. Yao, and L. Li, Structural, magnetic and magnetocaloric effect of $Gd_6(Mn_{1-x}Fe_x)_{23}$ compounds, J. Low Temp. Phys. **195**, 221 (2019).

[19] B. F. DeSavage, R. M. Bozorth, F. E. Wang, and E. R. Callen, Magnetization of the rare-earth manganese compounds R_6Mn_{23}, J. Appl. Phys. **36**, 992 (1965).

[20] H. R. Kirchmayr, Magnetic properties of rare earth manganese compounds, IEEE Trans. Magn. **2**, 493 (1966).

[21] H. R. Kirchmayr, Magnetic properties of the compound series $Y(Mn_xFe_{1-x})_2$ and $Y_6(Mn_xFe_{1-x})_{23}$, J. Appl. Phys. **39**, 1088 (1968).

[22] H. R. Kirchmayr and W. Steiner, Magnetic order of the compound series $RE_6(Fe_{1-x}Mn_x)_{23}$ (RE = Y, Gd), J. Phys. Colloq. **32**, C1-665 (1971).

[23] K. H. J. Buschow and R. C. Sherwood, Magnetic properties and hydrogen absorption in rare-earth intermetallics of the type RMn_2 and R_6Mn_{23}, J. Appl. Phys. **48**, 4643 (1977).

[24] S. K. Malik, T. Takeshita, and W. E. Wallace, Hydrogen induced magnetic ordering in Th_6Mn_{23}, Solid State Commun. **23**, 599 (1977).

[25] K. Hardman, W. J. James, J. Déportes, R. Lemaire, and R. Perrier de la Bâthie, Magnetic properties of R_6Mn_{23} compounds, J. Phys. Colloq. **40**, C5-204 (1979).

[26] W. J. James, K. Hardman, W. Yelon, and B. Kebe, Structural and magnetic properties of $Y_6(Fe_{1-x}Mn_x)_{23}$, J. Phys. Colloq. **40**, C5-206 (1979).

[27] A. Delapalme, J. Déportes, R. Lemaire, K. Hardman, and W. J. James, Magnetic interactions in R_6Mn_{23} rare earth intermetallics, J. Appl. Phys. **50**, 1987 (1979).

[28] K. H. J. Buschow, Magnetic properties of the ternary hydrides of Nd_6Mn_{23} and Sm_6Mn_{23}, Solid State Commun. **40**, 207 (1981).

[29] K. Hardman, J. J. Rhyne, and W. J. James, Magnetic structures of $Y_6(Fe_{1-x}Mn_x)_{23}$ compounds, J. Appl. Phys. **52**, 2049 (1981).

[30] F. T. Parker and H. Oesterreiche, Analysis of magnetic interactions and structure in R_6Mn_{23}, Appl. Phys. A **27**, 65 (1982).

[31] K. H. J. Buschow, P. C. M. Gubbens, W. Ras, and A. M. Van der Kraan, Magnetization and Mössbauer effect study of Dy_6Mn_{23} and Tm_6Mn_{23} and their ternary hydrides, J. Appl. Phys. **53**, 8329 (1982).

[32] H. Nagai, N. Oyama, Y. Ikami, H. Yoshie, and A. Tsujimura, The magnetic properties of psuedo-binary compounds, $Gd(Fe_{1-x}Mn_x)_2$ and $Gd_6(Fe_{1-y}Mn_y)_{23}$, J. Phys. Soc. Jpn. **55**, 177 (1986).

[33] H. Nagai, T. Yokoyama, S. Katsuyama, Y. Amako, H. Yoshiea, and K. Adachi, The anomalous behaviour of the electrical resistivities of $Gd(Fe, Mn)_2$ and $Gd_6(Fe, Mn)_{23}$, J. Magn. Magn. Mater. **177**, 1131 (1998).

[34] R. Coehoorn, Calculated electronic structure and magnetic properties of Y-Fe compounds, Phys. Rev. B **39**, 13072 (1989).

[35] H. J. Elmers, A. Chernenkaya, K. Medjanik, M. Emmel, G. Jakob, G. Schnhense, D. Gottlob, I. Krug, F. M. F. de Groot, and A. Gloskovskii, Exchange coupling in the correlated electronic states of amorphous GdFe films, Phys. Rev. B **88**, 174407 (2013).

[36] C. W. Chuang, F. M. F. de Groot, Y. F. Liao, Y. Y. Chin, K. D. Tsuei, R. Nirmala, D. Malterre, and A. Chainani, Hard x-ray photoemission spectroscopy of GdNi and HoNi, Phys. Rev. B **102**, 165127 (2020).

[37] *Hard X-ray Photoelectron Spectroscopy (HAXPES)*, edited by J. C. Woicik (Springer International Publishing, Switzerland, 2016), Vol. 59.

[38] J. Rodríguez-Carvajal, Recent advances in magnetic structure determination neutron powder diffraction, Phys. B: Condens. Matter **192**, 55 (1993).

[39] S. P. Kowalczyk, N. Edelstein, F. R. McFeely, L. Ley and D. A. Shirley, X-ray photoemission spectra of the 4*d* levels in rare-earth metals, Chem. Phys. Lett. **29**, 491 (1974).

[40] G. van der Laan, E. Arenholz, E. Navas, A. Bauer, and G. Kaindl, Magnetic circular dichroism and orbital momentum coupling in 4*d* photoemission from Gd(0001), Phys. Rev. B **53**, R5998(R) (1996).

[41] W. J. Lademan, A. K. See, L. E. Klebanoff, and G. van der Laan, Multiplet structure in high-resolution and spin-resolved x-ray photoemission from gadolinium, Phys. Rev. B **54**, 17191 (1996).

[42] J. Szade, M. Neumann, I. Karla, B. Schneider, F. Fangmeyer, and M. Matteucci, Photon energy dependence of the Gd 4*d* photoemission, Solid State Commun. **113**, 709 (2000).

[43] M. C. Biesinger, B. P. Payne, A. P. Grosvenor, L. W. M. Lau, A. R. Gerson, and R. St. C. Smart, Resolving surface chemical states in XPS analysis of first row transition metals, oxides and hydroxides: Cr, Mn, Fe, Co and Ni, Appl. Surf. Sci. **257**, 2717 (2011).

[44] R. T. Haasch, L. W. Martin, and E. Breckenfeld, Single crystal rare-earth scandate perovskites analyzed using x-ray photoelectron spectroscopy: 3. $GdScO_3(110)$, Surf. Sci. Spectra **21**, 149 (2014).

[45] J. Rusz, I. Turek, and M. Divis, Random-phase approximation for critical temperatures of collinear magnets with multiple sublattices: Gd*X* compounds (X = Mg, Rh, Ni, Pd), Phys. Rev. B **71**, 174408 (2005).

[46] M. Coldea, S. G. Chiuzbaian, M. Neumann, D. Todoran, M. Demeter, R. Tetean, and V. Pop, Magnetic and electronic properties of $GdNi_{5-x}Al_x$ intermetallic compounds, Acta Phys. Pol., A **98**, 629 (2000).

[47] V. Pop, M. Coldea, M. Neumann, S. Chiuzbaian, and D. Todoran, X-ray photoelectron spectroscopy and magnetism of Gd_3Ni_8Al, J. Alloys Compd. **333**, 1 (2002).

[48] A. Kowalczyk, A. Szajek, M. Falkowski, and G. Chelkowska, Magnetic properties and electronic structure of $GdNi_4Si$ compound, J. Magn. Magn. Mater. **305**, 348 (2006).

[49] M. Kwiecien, G. Chelkowska, and K. Rabijasz, Electronic structure, magnetic and electric properties of $Gd(Ni_{1-x}Co_x)_3$ compounds, J. Alloys Compd. **423**, 55 (2006).

[50] A. Bajorek, A. Chrobak, G. Chelkowska, and M. Kwiecien, Influence of Fe substitution on the structure and magnetic properties in $Gd(Ni_{1-x}Fe_x)_3$ intermetallic compounds, J. Alloys Compd. **485**, 6 (2009).

[51] A. Bajorek, A. Chrobak, K. Ociepka, and G. Chelkowska, The analysis of the magnetic properties and the electronic structure in the $Tb_xGd_{1-x}Fe_3$ intermetallics, Intermetallics **43**, 110 (2013).

[52] J. H. Van Vleck, The Dirac Vector Model in Complex Spectra, Phys. Rev. **45**, 405 (1934).

[53] P. S. Bagus, A. J. Freeman, and F. Sasaki, Prediction of New Multiplet Structure in Photoemission Experiments, Phys. Rev. Lett. **30**, 850 (1973).

[54] J. F. van Acker, Z. M. Stadnik, J. C. Fuggle, H. J. W. M. Hoekstra, K. H. J. Buschow, and G. Stroink, Magnetic moments and x-ray photoelectron spectroscopy splittings in Fe 3*s* core levels of materials containing Fe, Phys. Rev. B **37**, 6827 (1988).

[55] I. N. Shabanova, A. N. Maratkanova, and V. A. Sosnov, Satellites in core level XPS spectra of the Fe-based systems, J. Electron. Spectrosc. Relat. Phenom. **88–91**, 339 (1998).

[56] I. N. Shabanova, N. V. Keller, V. A. Sosnov, and A. Z. Menshikov, X-ray photoelectron studies of spin state changes in 3*d* metal systems, J. Electron. Spectrosc. Relat. Phenom. **114–116**, 581 (2001).

[57] L. Sangaletti, F. Parmigiani, and P. S. Bagus, Sum rule to evaluate the exchange energy in core-level photoemission, Phys. Rev. B **66**, 115106 (2002).

[58] P. S. Bagus, R. Broer, and E. S. Ilton, A new near degeneracy effect for photoemission in transition metals, Chem. Phys. Lett. **394**, 150 (2004).

[59] P. S. Bagus, E. S. Ilton, and C. J. Nelin, The interpretation of XPS spectra: Insights into materials properties, Surf. Sci. Rep. **68**, 273 (2013).